Turkish Journal of Electrical Engineering and Computer Sciences

Volume 24 | Number 5 Article 14

1-1-2016

Behavior of metamaterial-based microwave components for sensing and heating of nanoliter-scale volumes

MUHAMMED SAİD BOYBAY

Follow this and additional works at: https://journals.tubitak.gov.tr/elektrik

 Part of the Computer Engineering Commons, Computer Sciences Commons, and the Electrical and Computer Engineering Commons

Recommended Citation

BOYBAY, MUHAMMED SAİD (2016) "Behavior of metamaterial-based microwave components for sensing and heating of nanoliter-scale volumes," *Turkish Journal of Electrical Engineering and Computer Sciences*: Vol. 24: No. 5, Article 14. https://doi.org/10.3906/elk-1406-97
Available at: https://journals.tubitak.gov.tr/elektrik/vol24/iss5/14

This Article is brought to you for free and open access by TÜBİTAK Academic Journals. It has been accepted for inclusion in Turkish Journal of Electrical Engineering and Computer Sciences by an authorized editor of TÜBİTAK Academic Journals. For more information, please contact academic.publications@tubitak.gov.tr.

Turkish Journal of Electrical Engineering & Computer Sciences

http://journals.tubitak.gov.tr/elektrik/

Research Article

Turk J Elec Eng & Comp Sci
(2016) 24: 3503 – 3512
© TÜBİTAK
doi:10.3906/elk-1406-97

Behavior of metamaterial-based microwave components for sensing and heating of nanoliter-scale volumes

Muhammed Said BOYBAY[1,2,*]

[1]Department of Computer Engineering, Faculty of Engineering, Antalya International University, Antalya, Turkey
[2]Department of Mechanical and Mechatronics Engineering, University of Waterloo, ON, Canada

Received: 17.06.2014 • **Accepted/Published Online:** 03.05.2015 • **Final Version:** 20.06.2016

Abstract: Metamaterial-based microwave components are among the state-of-the-art heater and sensor designs for microfluidic systems. The miniaturization and energy-focusing abilities of the metamaterial-based components make it possible to adopt microwave components operating at wavelengths in the order of 10 cm for microfluidic systems. Microwave systems are particularly advantageous for point-of-care and high-throughput applications due to their high speed of operation, very low instrumentation cost, ability to selectively and internally heat specimens, and ability of label-free sensing. In this study, the efficiency and behavior of microwave components designed for heating and sensing small volumes in the scale of nanoliters are studied. In the heating behavior, an optimum passivation layer thickness that depends on the permittivity of the chip material is observed. Increasing the permittivity of the chip material increases the optimum passivation layer thickness. For a typical microfluidic environment that uses polydimethylsiloxane as the chip material and a lossy substrate, 37.4% of incoming microwave power is converted to heat within a 3-nL droplet. Increasing the permittivity of the chip material increases the heating efficiency. The sensing performance of the component shows that a 3-nL droplet generates a shift of 330 MHz (11.3%) in the resonance frequency. There is an optimum chip material permittivity that maximizes the shift in the resonance frequency. Increasing the passivation layer thickness reduces the sensitivity. Results provide a guideline for microwave heater and sensor designs in microfluidic platforms.

Key words: Microwave heating, microwave sensing, split ring resonator, microfluidics

1. Introduction

Microfluidics provide many advantages, including reduced reagent use, shortened reaction time, and increased sensitivity, for biological and chemical processes when compared with conventional techniques [1–3]. As a result, microfluidics find applications in lab-on-a-chip and point-of-care systems [4], micro total analysis systems [5], protein separation [6], DNA analysis [7], drug discovery [8], tissue engineering [9], etc. In order to fully realize the potential of microfluidic technology, one key need is to develop precise and fast systems for heating and sensing fluids within microchannels.

The majority of heaters in microfluidic systems are either conduction-based heaters or internal heaters. In the case of conduction-based heaters, heat is generated within the heater and conducted to the target naturally as a result of the generated temperature difference. Peltier modules, joule heating, and resistive heaters are samples of conduction-based heaters that are used in microfluidic systems [10–15]. In systems that are designed for fast and high-throughput analysis, conduction-based heaters do not provide enough heating speed and

*Correspondence: muhammed.boybay@antalya.edu.tr

material selectivity. On the other hand, in internal heaters such as optical [16,17] or microwave heaters [18], the heating mechanism is much faster and heat is generated within the target.

Similar to the need for new heater designs, localized, fast, and precise sensors are needed for microfluidic technology in order to realize compact lab-on-a-chip and high-throughput applications. In microfluidic systems sensors are mainly used for detecting or counting droplets and micro/nanoparticles. Optical [19], resistive [20,21], capacitive [22], and thermal [23] detection schemes are the most commonly used label-free sensing techniques. Major shortcomings of these techniques are expensive equipment, labor-intensive fabrication procedures due to alignment issues, and slow operation when compared to the operation speed of microfluidic devices.

Microwave heaters provide fast, selective, and cost-effective heating for microfluidic systems. The first microwave heater for microfluidic devices was reported in [24]. In [25,26], microwave heaters were employed for two-phase microfluidics and polymerase chain reaction operations, respectively. In a recent development, a fast and localized microwave component that can heat nanoliter droplets was developed by using metamaterial concepts [18]. The heater is able to heat the droplets one by one with a heating rate of 8 $^{\circ}$C/ms. In addition to the heating, the metamaterial-based component combines heating and sensing functions in a single unit.

In order to utilize advantages of microwave technology, e.g., cost-effective fabrication, ability of miniaturization, and reliable operation, in the design and fabrication of microwave components, the following requirements are necessary: 1) a planar design and fabrication procedure, 2) fabrication procedures for good conductors with trace height larger than the skin depth. Among the reported fabrication procedures, [18] is the only study that matches the requirements.

Although metamaterial-based microwave components for sensing and heating are demonstrated experimentally, their behavior under different material properties and chip designs has not been studied. For such a study, experimental methods are not well developed yet. A parametric experimental study of the effect of material properties is not possible since currently used materials for microfluidic systems are limited. In addition, procedures of planar microwave component fabrication for materials used in making microfluidic chips have not been developed except for polydimethylsiloxane (PDMS). The objective of this paper is to analyze sensing and heating performances of a metamaterial-based microwave component. The effect of microwave properties of chip material and substrate material is studied using numerical analysis. Resonance behavior of the heater and heat generation within a 3-nL droplet are analyzed.

2. Resonator structure and important parameters

The microwave component is composed of a ring resonator with a T-shaped capacitive gap, an excitation loop, and a coplanar transmission line that feeds the excitation loop as shown in Figure 1a. The energy dissipation from the structure can be classified in three categories: 1) conductive, 2) dielectric, and 3) radiative losses. In order to have an efficient heater for microfluidic platforms, the radiation loss must be reduced and dielectric loss must be concentrated within the channel. In this structure, the resonator concentrates the **E** field energy within the capacitive gap, which has a foot print of 200 μm $\times$ 120 μm. Figure 1b presents a side view of the structure.

The lumped element model of the structure is presented in Figure 2. L_{outer} and R_{outer} represent inductance and total resistance that includes the conductive and radiative losses of the excitation loop, respectively. The inner split ring resonator (SRR) has an inductance of L_{SRR} due to the current circulation, a resistance of R_{Cu} due to the conductive losses, a resistance of R_r due to radiation, a capacitance of C_{SRR} due to the T-shaped gap, and a resistance of R_d as a result of the dielectric loss within the capacitance.

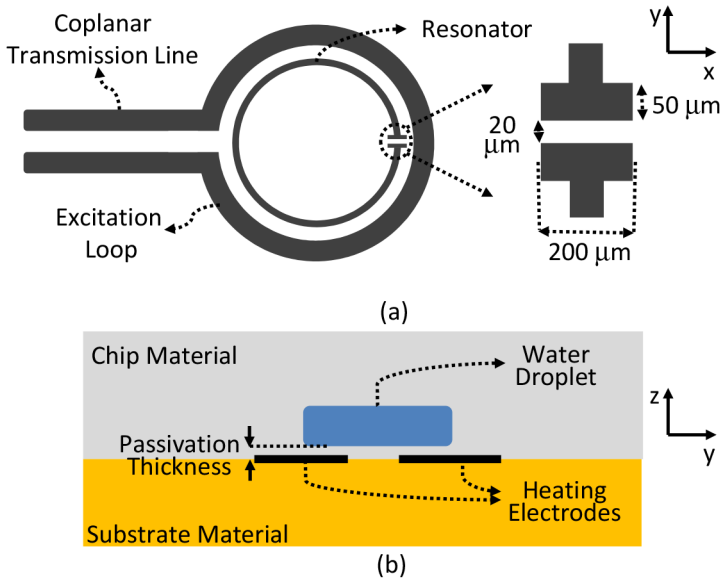

Figure 1. (a) Top view of the heater including the excitation structure and the resonator. Same dimensions as presented in [18] are used for comparison purposes. (b) Side view of the heating zone. The electrodes are covered by a passivation layer to prevent short circuit and contamination. Water droplets have the dimensions of 300 μ m $\times$ 200 μ m $\times$ 50 μ m.

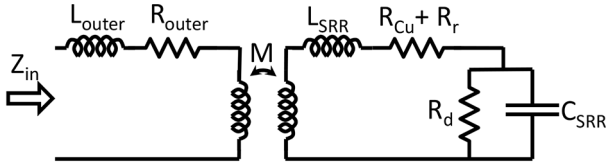

Figure 2. Circuit model for the sensing and heating element. Z_{in} is the impedance observed by the coplanar transmission line (see Figure 1). Variations in C_{SRR} indicate a change in the dielectric constant of the fluid and variations in R_d indicate a change in the imaginary part of the permittivity of the fluid. Power dissipated within R_d is converted to heat.

The input impedance of such a circuit is given by:

$$Z_{in} = R_{outer} + j\omega L_{outer} + \frac{\omega^2 M^2}{Z_r}, \tag{1}$$

where

$$Z_r = R_{Cu} + R_r + j\omega L_{SRR} + \frac{R_d}{1 + j\omega C_{SRR} R_d} \tag{2}$$

In a typical microfluidic system, usually a chip that contains the microfluidic channel is bonded on a substrate (Figure 1b). In order to analyze the effect of material selection on the heating and sensing performance, the behavior of the microwave component is studied for different permittivity and loss tangent values. Chip and substrate material combinations that are presented in the Table are selected to cover frequently used materials in microfluidic chips and to investigate limitations and characteristics of the component. Typically, glass, PDMS (ε = 2.5–2.7, $\tan\delta$ = 0.01–0.04 [27]), polymethylmethacrylate (PMMA), and quartz are used in chip fabrication.

Table. Combinations of substrate and chip materials.

Case #	1	2	3	4	5	6	7	8	9	10
ε_{subs}	5.5	5.5	5.5	5.5	5.5	5.5	5.5	5.5	5.5	5.5
$\tan\delta_{subs}$	0	0.005	0.01	0.01	0.01	0.01	0.01	0.01	0.01	0.01
ε_{chip}	1	1	1	1.5	2.5	3.4	5.5	10	2.5	2.5
$\tan\delta_{chip}$	0	0	0	0	0	0	0	0	0.02	0.04

In addition to material properties, passivation layer thickness (d) is also an important parameter. The passivation layer is required in almost all microfluidic systems that use electrodes. The main reasons behind the use of a passivation layer are to prevent contamination, to generate well-defined droplets, and to prevent short circuits if capacitive electrodes are being used. The interaction of the droplet with the electric field generated by the capacitive gap depends on the distance between the electrodes and the droplet. As a result, the effect of the droplet on C_{SRR} is a function of d. Due to the fabrication processes reported in [18], d cannot be controlled precisely. Therefore, full-wave numerical analysis is used to analyze the effect of d on the performance. All of the structure including the coaxial to coplanar transmission line transition via an edge mount SMA connector (Emerson Connectivity Part # 142-0701-841) is modeled in the simulator.

Figure 3 presents typical behavior of the heater for different d values for Case 1. The reflection coefficient presents a clear resonance frequency (f_r) around 3 GHz. Since the chip material is assumed to be in a vacuum, as the water droplet becomes closer to the electrodes, the capacitance increases. As a result f_r shifts to higher frequencies as the passivation layer increases. For Case 1, as d changes from 2 μ m to 20 μ m, a shift of 275 MHz in f_r is observed, which corresponds to a dielectric constant change from 1 to 81.

At the resonance frequency, the operation wavelength is around 10 cm. Since the outer diameter of the excitation loop is 6.45 mm [18], the size of the resonator structure is comparable to the operation wavelength. As a result, radiation characteristics of the structure must be analyzed to ensure that the structure is not radiating efficiently. Figure 4 presents radiated power as a function of frequency for Case 1. The radiated power increases exponentially until the resonance frequency is reached. When the structure is excited by a 1-W source, the radiated power as a function of frequency is given by:

$$P_r = \left(0.02e^{f/0.89} - 0.022\right) W \tag{3}$$

where f is the operation frequency in GHz. At the resonance frequency the radiated power is reduced significantly, typically below 20%, and it is further reduced as the passivation layer thickness increases (around 10% when d = 20 μ m).

3. Sensing performance

When a water droplet is present near the capacitive region of the microwave component, due to the contrast between the microwave properties of the droplet and the chip material, the reflection coefficient changes. The loss tangent of the water droplet affects R_d and the permittivity of the droplet affects C_{SRR}. Therefore, the loss tangent of the droplet mainly affects the quality factor of the resonator and the dielectric constant affects the resonance frequency. The change in the resonance frequency due to a change in the permittivity is given by [28]:

$$\frac{f_{r1} - f_{r2}}{f_{r1}} = \frac{\int_v \left(\Delta\varepsilon \mathbf{E_1}\cdot\mathbf{E_0}\right) dv}{\int_v \left(\varepsilon \left|E_0\right|^2 + \mu_0 \left|H_0\right|^2\right) dv} \tag{4}$$

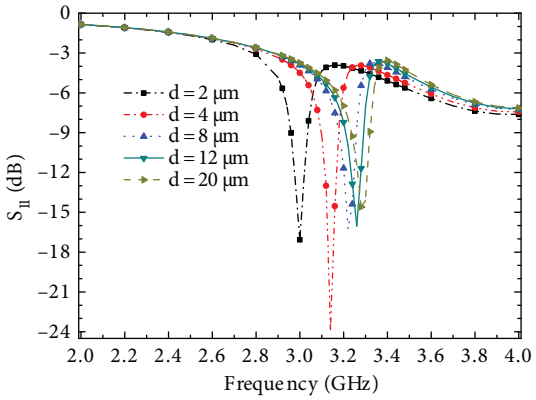

Figure 3. Reflection coefficient as a function of frequency for Case 1.

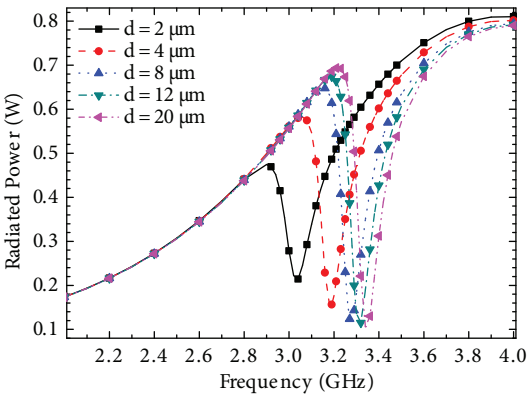

Figure 4. Radiated power as a function of frequency for where Case 1 with a total excitation power of 1 W.

$\Delta\varepsilon$ is the change in the permittivity, v is the perturbed volume, f_{r1} is the resonance frequency before the perturbation, and f_{r2} is the resonance frequency after the perturbation. $\mathbf{E_0}$ and $\mathbf{H_0}$ are the field distributions without the perturbation and $\mathbf{E_1}$ and $\mathbf{H_1}$ are the field distributions with the perturbation.

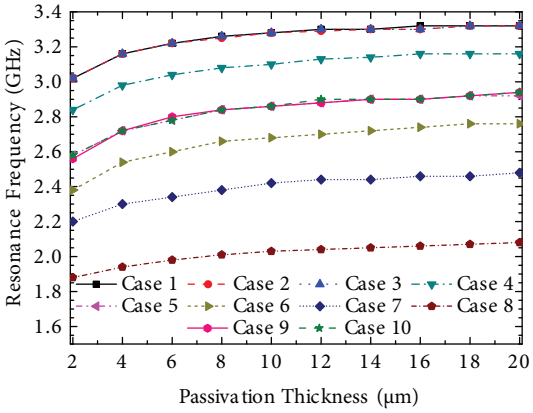

Figure 5. f_r as a function of d for different material combinations. As the permittivity of the dielectric constant increases, f_r reduces. The loss tangent of the chip material does not have a considerable effect on f_r.

In Figure 5, f_r as a function of d is presented. Results for Cases 1, 2, and 3 and Cases 5, 9, and 10 show that loss tangents of the substrate ($\tan\delta_{subs}$) and chip material ($\tan\delta_{chip}$) have minor effects on f_r. On the other hand, the permittivity of the chip material (ε_{chip}) reduces f_r by increasing the capacitance of the resonator (Cases 3–8). As d increases, resonance frequency saturates. For d >16 μ m, changing d does not affect the resonance frequency considerably.

In order to quantify the sensitivity of f_r to d, change in the resonance frequency (Δf_r) is calculated. Δf_r, defined as

$$\Delta f_r = f_r|_{d=20\mu m} - f_r|_{d=2\mu m} \tag{5}$$

is presented in Figure 6 as a function of ε_{chip}. A sensitivity peak at $\varepsilon_{chip} = 2.5$ is observed as a result of the composition of C_{SRR}. C_{SRR} is composed of two parallel capacitances, $C_{SRR} = C_{glass} + C_{chip}$. The first capacitance, C_{glass}, is constant and is due to the **E** field within the glass substrate and air under the electrodes (–z direction in Figure 1b). The second capacitance, C_{chip}, is due to the **E** field within the chip material and

the droplet (+z direction in Figure 1b) and is the varying capacitance that actually senses the droplet. At low ε_{chip} values, increasing ε_{chip} increases the contribution of C_{chip} in C_{SRR}. As a result, changes in C_{chip} result in a higher frequency shift. On the other hand, since higher ε_{chip} reduces the permittivity contrast between water and the chip material, the sensitivity reduces when ε_{chip} is increased further. Eventually the frequency shift is expected to become zero as ε_{chip} approaches the dielectric constant of water.

4. Heating performance

In order to analyze the efficiency of the heater, the power dissipated within the water droplet is calculated. Since water does not have a magnetic response, the dissipated microwave power within the droplet can be written as:

$$P_{heat} = \int_V (\mathbf{J}^* \cdot \mathbf{E})\, dv \tag{6}$$

where **J** is the current density, **E** is the electric field, and V is the volume of the droplet.

Figure 7 presents a typical behavior of the heat generation within the droplet as a function of frequency when 1 W of power is used. At resonance frequencies the heat generation is maximum. For Case 1, as d increases, heat generation within the droplet reduces and 40% of the input power is converted to heat within the droplet for d = 2 μ m.

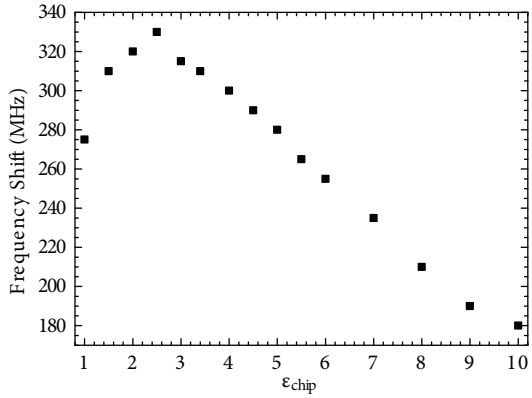

Figure 6. Frequency shift as a function of permittivity of the chip material. The substrate is assumed to be glass with a loss tangent of 0.005. Frequently used materials in microfluidic systems are indicated in the plot.

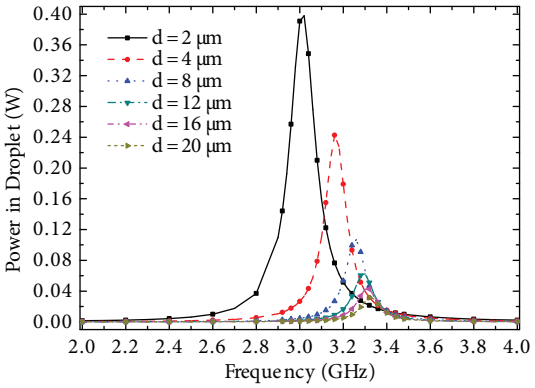

Figure 7. The microwave power dissipated in water as a function of frequency for different d values. The material combination of Case 1 is used.

An important feature of the microwave heating using the metamaterial concept is selective heating. Since the material and the size of the droplet affect the resonance frequency, the heater operates at different frequencies for different droplets. For selectivity, full width at half maximum (FWHM) is an important parameter. FWHM for the heat generation is between 140 MHz and 120 MHz. In other words, if the heater is tuned to droplets with specific size and material content, the heat generation within a different droplet will be reduced by more than 50% if the different droplet shifts the resonance frequency by more than 70 MHz.

4.1. Effect of $\tan\delta_{subs}$

Figure 8 presents the effect of $\tan\delta_{subs}$ on the heat generation within the droplet. Compared to the lossless case, $\tan\delta_{subs} = 0.005$ reduces the heat generation by 13.3% for d = 2 μ m. As d increases the reduction in the

heat generation within the droplet due to $\tan\delta_{subs}$ increases. An average of 19.8% reduction in heat generation is observed when $10 \leq d \leq 20$. When $\tan\delta_{subs}$ is doubled, the heat generation is further reduced, but the reduction is not doubled. For $d = 2\ \mu$ m, a substrate with $\tan\delta_{subs} = 0.01$ reduces the heat generation by 25%. For $10 \leq d \leq 20$, reduction in heat generation is almost constant with an average of 34.6% and standard deviation of 1.09%.

The effect of the loss tangent of the substrate is tolerable for medium loss values and for low passivation layer thicknesses. Although $\tan\delta_{subs}$ does not completely suppress the heating mechanism, low-loss glass is the proper substrate material for heating applications unless a flexible substrate is required.

4.2. Effect of ε_{chip}

Figure 9 analyzes effect of ε_{chip} on the heating performance by comparing Cases 3–8. The first important observation is that when ε_{chip} increases, heat generation increases. This response is attributed to two factors. The first one is the behavior of C_{SRR} as discussed in Section 3: higher ε_{chip} concentrates more of the capacitive energy within the chip and droplet rather than within the glass substrate. The second is the behavior of evanescent waves in dielectric media. The field generated by the microwave component is a superposition of radiative and evanescent waves [29]. Since the radiation efficiency is very low at the resonance frequency, the field is dominated by the evanescent waves. As the permittivity of a medium increases, the decay constant of evanescent fields becomes smaller and fields become more diverged.

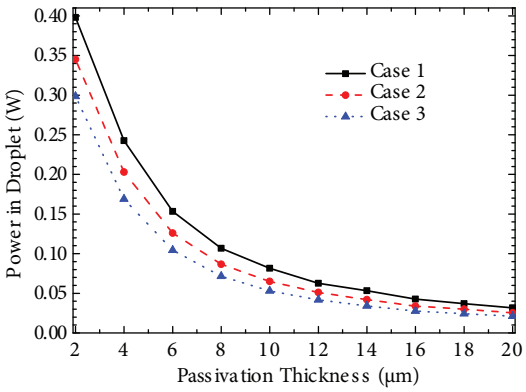

Figure 8. Heat generation within the droplet as a function of d for different $\tan\delta_{subs}$ under 1 W of excitation power.

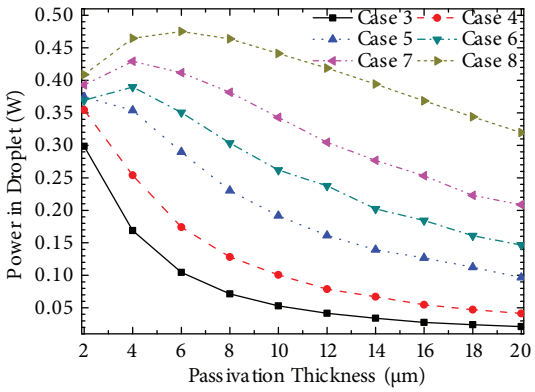

Figure 9. Maximum power deposition as a function of d for different material combinations. The effect of the permittivity of the chip material on the heating characteristic is presented.

Another important and yet counterintuitive result is that heat generation is not reduced monotonically as d increases. On the other hand, a monotonically decreasing behavior is expected since the **E** field decays in the z direction due to the behavior of evanescent fields. Figure 9 shows that although at low ε_{chip} values, heat generation is reduced monotonically, at higher ε_{chip} values, an optimum passivation layer thickness is observed at which the heat generation within the droplet is maximized. This behavior is a result of the entangled relationship between the quality factor of the resonator, **E** field strength, and d. For example, in Case 8, at $d = 2\ \mu$ m, the resistance of the resonator is high and as a result the quality factor is low. A low quality factor deteriorates matching and reduces the strength of the **E** field. As d increases, the resistance is reduced and a better matching is achieved, which increases the heat generation within the droplet. Further increasing d makes

the quality factor even better, but since R_d becomes smaller (or the droplet becomes far away from the heating zone), the heat generation reduces. This behavior can be observed in Figure 10 where the reflection coefficient as a function of frequency is presented for Case 8.

4.3. Effect of $\tan\delta_{chip}$

In order to analyze the effect of $\tan\delta_{chip}$, maximum heat generation is plotted as a function of passivation layer thickness for Cases 5, 9, and 10 in Figure 11. Among the frequently used materials in microfluidic channels, PDMS has the highest loss tangent. Therefore, different loss tangent values for PDMS material are analyzed. Increasing the loss tangent reduces the heat generation within the droplet. For the typical value of $\tan\delta_{chip} = 0.02$, the efficiency is reduced by 17.9% for d $= 2$ μ m. As d increases, the reduction in heat generation within the droplet increases and at d $= 20$ μ m a reduction of 27.3% is observed.

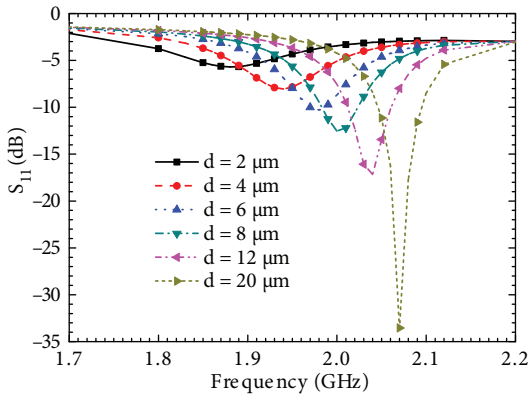

Figure 10. Reflection coefficient as a function of frequency for Case 8. Increasing d increases the quality factor.

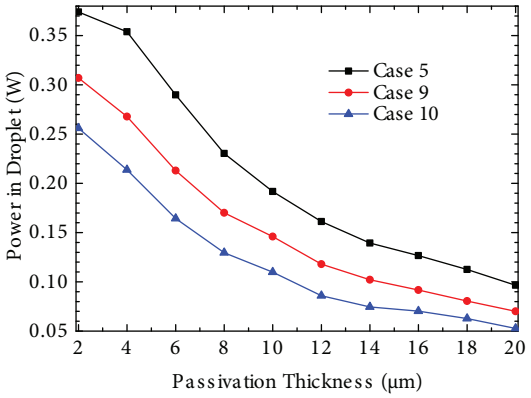

Figure 11. Maximum power deposition as a function of d for different material combinations. The effect of the loss tangent of the chip material on the heating characteristic is presented.

5. Comparison with experimental data

Although a parametric experimental study is not available in the literature, the experimental data presented in [18] can be used for comparison purposes. Droplets were generated within a 200 μ m $\times$ 50 μ m channel. Lengths of the droplets varied between 300 μ m and 400 μ m. The chip material was PDMS (Sylgard 184, Dow Corning) and the passivation layer was hard PDMS (EG-6301, Dow Corning). Although a consistent passivation layer thickness fabrication was not demonstrated, chips used for the experimentations had passivation layer thicknesses between 5 μ m and 10 μ m. Finally, a low-loss glass substrate was used for fabrication.

In [18], the heating experiments show that 0.647 mJ heat is generated within the droplet in 5.62 ms, under 0.5 W of excitation power. These values correspond to a 23.03% efficiency in depositing energy to the droplet. For the sensing performance, a resonance frequency of 120 MHz was observed for droplets. According to Figure 11, 23.03% efficiency corresponds to an interval of passivation layer thickness between 3.2 μ m and 8 μ m. According to Figure 5, for PDMS chip material (Cases 5, 9, and 10), a Δf_r of 120 MHz corresponds to a d value between 6 μ m and 8 μ m. Therefore, the experimental data presented in [18] are consistent with the numerical analysis presented in this work.

6. Conclusion

Effects of the passivation layer and electromagnetic properties of materials employed in microfluidic systems on the behavior and efficiency of microwave components are analyzed. The sensing behavior of the microwave component reveals that at a certain chip material permittivity the sensitivity is maximized. For a 3-nL water droplet, a 330-MHz resonance frequency shift is achieved.

The passivation layer thickness, or in other words the distance between the water droplet and the electrodes, affects both the quality factor of the resonator and heat generation within the droplet. As a result, in the case of chip materials with high permittivity, an optimum passivation layer thickness where the efficiency is maximized is observed. Although increasing the loss tangent of the substrate and chip material reduces the efficiency, heating efficiency of more than 25% is achieved even with high substrate and chip material losses.

Acknowledgment

This work was supported by the Scientific and Technological Research Council of Turkey under Grant # 113E135.

References

[1] Janasek D, Franzke J, Manz A. Scaling and the design of miniaturized chemical-analysis systems. Nature 2006; 442: 374-380.

[2] deMello AJ. Control and detection of chemical reactions in microfluidic systems. Nature 2006; 442: 394-402.

[3] Beebe DJ, Mensing GA, Walker GM. Physics and applications of microfluidics in biology. Annu Rev Biomed Eng 2002; 4: 261-286.

[4] Kim U, Ghanbari S, Ravikumar A, Seubert J, Figueira S. Rapid, affordable, and point-of-care water monitoring via a microfluidic dna sensor and a mobile interface for global health. IEEE J Transl Eng Health Med 2013; 1: 3700207.

[5] Culbertson CT, Mickleburgh TG, Stewart-James SA, Sellens KA, Pressnall M. Micro total analysis systems: fundamental advances and biological applications. Anal Chem 2014; 86: 95-118.

[6] Shameli SM, Glawdel T, Fernand VE, Ren CL. Micellar affinity gradient focusing in a microfluidic chip with integrated bilinear temperature gradients. Electrophoresis 2012; 33: 2703-2710.

[7] Abate AR, Hung T, Sperling RA, Mary P, Rotem A, Agresti JJ, Weiner MA, Weitz DA. DNA sequence analysis with droplet-based microfluidics. Lab Chip 2013; 13: 4864-4869.

[8] Neužil P, Giselbrecht S, Länge K, Huang TJ, Manz A. Revisiting lab-on-a-chip technology for drug discovery. Nat Rev Drug Discov 2012; 11: 620-632.

[9] Huh D, Hamilton GA, Ingber DE. From 3{D}cell culture to organs-on-chips. Trends Cell Biol 2011; 21: 745-754.

[10] Liu RH, Yang J, Lenigk R, Bonanno J, Grodzinski P. Self-contained, fully integrated biochip for sample preparation, polymerase chain reaction amplification, and DNA microarray detection. Anal Chem 2004; 76: 1824-1831.

[11] de Mello AJ, Habgood M, Lancaster NL, Welton T, Wootton RCR. Precise temperature control in microfluidic devices using Joule heating of ionic liquids. Lab Chip 2004; 4: 417-419.

[12] Maltezos G, Johnston M, Scherer A. Thermal management in microfluidics using micro-Peltier junctions. Appl Phys Lett 2005; 87: 154105.

[13] Lee CY, Lee GB, Lin JL, Huang FC, Liao CS. Integrated microfluidic systems for cell lysis, mixing/pumping and DNA amplification. J Micromech Microeng 2005; 15: 1215-1223.

[14] Vigolo D, Rusconi R, Piazza R, Stone HA. A portable device for temperature control along microchannels. Lab Chip 2010; 10: 795-798.

[15] Kaigala GV, Hoang VN, Stickel A, Lauzon J, Manage D, Pilarski LM, Backhouse CJ. An inexpensive and portable microchip-based platform for integrated RT-PCR and capillary electrophoresis. Analyst 2008; 133: 331-338.

[16] Kim H, Dixit S, Green CJ, Faris GW. Nanodroplet real-time PCR system with laser assisted heating. Opt Express 2009; 17: 218-227.

[17] Baroud CN, de Saint Vincent MR, Delville JP. An optical toolbox for total control of droplet microfluidics. Lab Chip 2007; 7: 1029-1033.

[18] Boybay MS, Jiao A, Glawdel T, Ren CL. Microwave sensing and heating of individual droplets in microfluidic devices. Lab Chip 2013: 13: 840-3846.

[19] Tkaczyk AH, Tkaczyk ER, Norris TB, Takayama S. Microfluidic droplet consistency monitoring and encapsulated cell detection via laser excitation. J Mech Med Biol 2011; 11: 1-14.

[20] Gawad S, Schild L, Renaud P. Micromachined impedance spectroscopy flow cytometer for cell analysis and particle sizing. Lab Chip 2001; 1: 76-82.

[21] Wang F, Burns MA. Multiphase bioreaction microsystem with automated on-chip droplet operation. Lab Chip 2010; 10: 1308-1315.

[22] Elbuken C, Glawdel T, Chan D, Ren CL. Detection of microdroplet size and speed using capacitive sensors. Sensor Actuat A-Phys 2011; 171: 55-62.

[23] Vutha KM, Davaji B, Lee CH, Walker GM. A microfluidic device for thermal particle detection. Microfluid Nanofluid 2014; 17: 871-878.

[24] Shah JJ, Sundaresan SG, Geist J, Reyes DR, Booth JC, Rao MV, Gaitan M. Microwave dielectric heating of fluids in an integrated microfluidic device. J Micromech Microeng 2007; 17: 2224-2230.

[25] Issadore D, Humphry KJ, Brown KA, Sandberg L, Weitz DA, Westervelt RM. Microwave dielectric heating of drops in microfluidic devices. Lab Chip 2009; 9: 1701-1706.

[26] Shaw KJ, Docker PT, Yelland JV, Dyer CE, Greenman J, Greenway GM, Haswell SJ. Rapid PCR amplification using a microfluidic device with integrated microwave heating and air impingement cooling. Lab Chip 2010; 10: 1725-1728.

[27] Farcich NJ, Salonen J, Asbeck PM. Single-length method used to determine the dielectric constant of polydimethylsiloxane. IEEE T Microw Theory 2008; 56: 2963-2971.

[28] Pozar DM. Microwave Engineering. 3rd ed. Hoboken, NJ, USA: Wiley, 2005.

[29] Harrington RF. Time-Harmonic Electromagnetic Fields. New York, NY, USA: McGraw-Hill, 1961.